Fermi National Accelerator Laboratory

FERMILAB-FN-607

Selected Topics in Sampling Calorimetry

Dan Green

Fermi National Accelerator Laboratory
P.O. Box 500, Batavia, Illinois 60510

September 1993

Operated by Universities Research Association Inc. under Contract No. DE-AC02-76CHO3000 with the United States Department of Energy

Disclaimer

SELECTED TOPICS IN SAMPLING CALORIMETRY

Dan Green

Fermi National Accelerator Laboratory
Batavia, Illinois 60510

September 1993

1. Introduction and Basic Concepts

This note attempts to make a selective overview of sampling calorimetry. The selection of topics is not meant to be inclusive. Many very good inclusive reviews already exist[1]. The goal here is to highlight and feature some few areas of topical interest within the purview of sampling calorimetry.

1.1 Scales, Xo and Ec for e Response

A particle incident upon a calorimeter deposits energy. The mechanism for the energy deposit is a cascade process. The longitudinal scale for the deposition in the case of electromagnetic (EM) interactions is the radiation length, Xo, defined in Eq. 1a. Particles continue to multiply until they reach the critical energy, Ec, following which they lose energy by ionization. At the critical energy the ionization loss is as given in Eq. 1b;

$$(dE/E)_{RAD} = -dx/Xo,\ Xo \sim \left[180\left(gm/cm^2\right)\right]\left[A/Z^2\right]$$
$$t = x/Xo \tag{1a}$$

$$(dE/dx) = -Ec/Xo,\ (dE/dx)_{mip} \sim \left[3\left(gm/cm^2\right)\right]\left[Z/A\right]$$
$$Ec \sim \left[550(MeV)\right]\left[1/Z\right] \tag{1b}$$
$$y = E/Ec$$

The natural distance unit is t, in Xo units, while the natural energy unit is y in Ec units. The Xo value scales as A/Z^2, while Ec scales as 1/Z. For example, Pb has Ec ~ 7 MeV, $(dE/dx)_{mip}$ ~ 1.1 MeV/gm/(cm^2), and Xo=0.56 cm.

1.2 Scales, λo and Et for Pionic Response

An analogous situation obtains for hadrons. The cascade is characterized longitudinally by the nuclear absorption length, λo, and the shower multiplication continues until the pion production threshold, Et, is reached. A complication is that the hadronic interaction creates neutral and charged pions, with neutral fraction fo. The neutral pions then drop out of the hadronic cascade and propagate as an EM shower component to which the calorimeter may respond, as e, differently

from its hadronic response, h. Note that fo, as defined, implies averaging over all cascade generations.

$$\begin{aligned} &\lambda o \sim \left[35\left(gm/cm^2\right)\right]\left[A^{1/3}\right] \\ &\mathrm{v} = x/\lambda o \\ &E = \left[efo + h(1-fo)\right]E_{in} \\ &Et \sim 2m_{\pi} \sim 0.28\ MeV \\ &< n > \sim \ell n(E) \end{aligned} \tag{2}$$

For example, in Fe, λo is ~ 132 gm/(cm2) or 16.76 cm. In Pb, Xo/λo is ~ 3.3%, so that EM and hadronic showers will develop very differently in depth.

The neutral fraction, summed over the entire hadronic shower, increases with hadron energy, being fo ~ 50% at 10 GeV. This increase is due to the increase of pion multiplicity with energy and the irreversible nature of neutral pion production. Clearly, as $E \to \infty, fo \to 1$.

The EM cascades vary little from event to event save in the location of the conversion point. For hadrons, the initiation point varies, as does the neutral fraction, and the nuclear excitation. Hadronic showers are much more variable. A sample from the HF data[2] is shown in Fig.1.

1.3 Showers and Particle Production

An extremely simplified model provides physical insight into the cascade process. Define e(t) as the typical shower energy at depth t, which has undergone t generations of cascade, each generation causing the number of shower particles to increase by a factor 2;

$$e(t) \sim E/2^t,\ n(t) = 2^t,\ t\max \sim \ell n(y),\ n(t\max) \sim E/Ec = y \tag{3}$$

Clearly, the shower stops multiplying when the particle energy is ~ Ec. That occurs at a "shower max", = SM, depth ~ ℓn(y). Clearly, a calorimeter is a linear device, n(tmax) ~ E, and statistical fluctuations in the number of shower particles imply that there is a "stochastic term", with coefficient a, in the energy resolution;

$$dE/E = a/\sqrt{E} \oplus b \tag{4}$$

In general, nonuniformities will also cause a "constant term", b, which will be folded in quadrature with the stochastic term caused by statistical error. Several nonuniformities will be discussed later in this note, along with the "induced constant term" which they generate.

A plot of dE/E as a function of $1/\sqrt{E}$ for HF data[2] is shown in Fig. 2. The expected decrease of dE/E with $\sqrt{E}$ is seen.

Obviously, the # of independent particles is limited by the end of multiplication. The total "path length", = L, (in Xo units) is $L = \int_0^{t\max} n(t)dt$ or $L \sim (E/Ec)/\ell n2$. Therefore, the hadronic resolution must be worse than the EM resolution, $a_{\pi}/a_e \sim \sqrt{Et/Ec} \sim 6$. As will be shown, the data roughly supports this expectation.

1.4 Longitudinal, 1-D Shower Development

To lowest order, the shower may be considered to be 1 dimensional, since the physical processes are characterized by very limited transverse momenta;

$$< Pt >_e \sim m_e, < Pt >_\pi \sim 300\ MeV \tag{5}$$

For EM showers, there is a fast rise due to multiplication, u^c, and a falloff due to ionization, e^{-u}, when e(t) < Ec. A reasonable parametrization of the EM shower is[3];

$$(dE/E)_e = du\left[u^c e^{-u}\right]/\Gamma(c+1),\ u = dt,\ d \sim 0.5,\ c \sim \ell n(y) \sim t\max \tag{6}$$

The SM location scales as ~ℓn(y), as before. That means that there are Z dependent differences in the shower, since y ~ 1/Ec ~ Z.

The shower particle mean free path (mfp) at e(t) ~ Ec is ~ 1/d in Xo units, looking at Eq. 6. In Pb a photon with energy = Ec has a mfp of 10 gm/(cm^2) which is 1.6 Xo, as expected.

For hadrons, there is an EM and hadronic piece of the shower. A 2 component parametrization[4] of the hadronic shower is;

$$(dE/E)_\pi = du\left[u^c e^{-u} fo\right]/\Gamma(c+1) + dw\left[w^g e^{-w}(1-fo)\right]/\Gamma(g+1)$$
$$w = gv,\ g \sim 1 \tag{7}$$

The EM part is similar to Eq. 6, while the hadronic piece is similar in form, but with a length scale = v, as expected. Note that the falloff in the hadronic shower has a mfp length scale ~ λo. For example, a pion with energy = Et has a range 100 gm/(cm^2) in Fe, while λo is 132 gm/(cm^2).

The integral neutral fraction, fo, is ~ 1/2 as mentioned above. A simple model for fo can be made. Consider a cascade with multiplication <n>, constant, per generation. Assume that $"fo" = 1/3 = \pi^o/\left(\pi^+ + \pi^o + \pi^-\right)$ for each generation. Then the shower neutral energy fraction is;

$$fo = "fo"\left[\sum_{v=0}^{(v\max^{-1})}(1-\text{fo})^v\right],\quad \text{vmax} = \ell n(E/Et)/\ell n(< n >) \tag{8}$$

Clearly, for 1 generation fo = "fo", while for $v\max \to \infty, fo \to 1$ as expected. For example, for 3 generations, if "fo" = 1/3, then fo ~19/27.

2. Sampling - Lowest Order

2.1 Sampling Error

This completes the preliminaries. A sampling calorimeter, where the shower is developed in a series of plates of thickness, Δt or Δv, performs the detection of cascade energies in a corresponding series of active plates of small thickness. Assuming that there is no correlation between the particles crossing the active layers, one can estimate the "stochastic" term due to statistical fluctuations in the active plate counts. If Nc is the total number traversing all active

layers, then $dE/E \sim 1/\sqrt{N_C}$. Since L ~ E/Ec, clearly, N_C ~ (E/Ec)/Δt. The error due to the fluctuation in the fraction of the energy appearing in the active layers is then;

$$a_e \sim \sqrt{\Delta t E c} \sim \sqrt{\Delta E}$$
$$a_\pi \sim \sqrt{\Delta v E t} \qquad (9)$$

Note that, since the ionization loss is as given in Eq.1b, the energy lost by a "mip" in the absorber layer is ~ EcΔt. Therefore, the stochastic term may alternatively be written as $a_e \sim \sqrt{\Delta E}$, where ΔE is the energy loss per sampling layer. Clearly, as the sampling becomes finer, the sampling error approaches zero at this level of approximation.

For example, for a 1 GeV e shower in Pb, Ec = 7.4 MeV, so with sampling at 1/2 Xo, one expects n(tmax) = 131, N_C = 262, and a_e = 6.2%. By comparison, for a 1 GeV hadron shower with 1/2 λo sampling, n(tmax) = 3.6, N_C = 7.2 and a_π = 37%.

HF data[2] for incident pions was used to change the sampling fraction in software. The results are shown in Fig. 3. For hadrons the unfolded result is $150\%\sqrt{\Delta v}$. The expected statistical behavior, sqrt(sampling thickness) is clearly seen, although the magnitudes are somewhat high due to the existence of other statistical error sources. The HF data is in good agreement with the other data shown in Fig. 3.

2.2 Threshold Effects, Other Statistical Errors

It has been assumed that all particles in the cascade are detectable. If the # of detectable particles is reduced by a "threshold" for detection, the stochastic term will clearly be increased. For example, Cerenkov light emission by electrons in the cascade has a threshold of e(t) > 1 MeV for Pb glass detectors. The increase in stochastic term is defined to be, $a \to a/\sqrt{F(\delta)}$, where for a threshold Eth >> Ec, F → 0, while if Eth << Ec, F → 1. The factor F is a function of $\delta \sim Eth/Ec$, and is tabulated in the references[1]. As an example, for Eth/Ec = 0.2, F ~ 0.5, causing a ~ 25% increase in the stochastic term.

Other statistical fluctuations may be important. For example, if the signal is produced using photomultiplier tubes, a device with 200 photoelectrons/GeV would contribute an additional 7% stochastic term, which would fold in quadrature with the 6% term found for 1/2 Xo Pb sampling, causing a ~ 40% increase in the total stochastic term. Clearly, the readout should have sufficient statistics so as not to contribute substantially to the intrinsic device resolution.

2.3 Binding Energy Losses

For hadronic showers there are additional complications. The EM shower involves the nucleus in bremmstrahlung and pair production with very small momentum transfers. Thus, the nucleus remains intact. For pions this is not true, and the nucleus is disrupted (see Eq. 5.). This process of disruption leads to fluctuations. The fraction of incident energy going into "binding energy" nuclear fragments is ~ 30%, and the fluctuations are large. The resulting "binding energy stochastic coefficient" is ~ 20%, although the details depend critically on the precise construction of the calorimeter[5]. Other fluctuations are due to neutrino or muon losses due to the decays of pions in the cascades.

2.4 Effects Due to e/h ≠ 1

As noted in Eq. 2, the hadronic cascade has an EM and a hadronic part. If the calorimeter responds differently to the 2 components, the fluctuations in the EM fraction, fo, will cause an "induced constant term" due to "non-compensation"[6], as can be easily seen by differentiating Eq. 2.

$$(dE/E)_{fo} \sim |e/h - 1| dfo$$
$$dfo \sim d\,"fo"\sqrt{< n_{\pi o} >}/< n_{\pi} > \qquad (10)$$

Assuming that the main error comes from the statistics of the first interaction (in analogy to the first dynode of a PMT), one can see that this effect decreases with incident energy as $1/\sqrt{\ell n(E)}$, since particle production goes as, $< n > \sim \ell n(E)$, Eq. 2. For example, for E = 200 GeV, with <n> = 9, there are only 3 π^o produced in the first interaction. This means that d"fo" = 0.17, so that a calorimeter with a 20% difference in response to the EM and hadronic shower components, e/h = 1.2, has a 3.5% induced constant term in the energy resolution dE/E. This rough estimate is in reasonable agreement with sophisticated models[7].

Note that, since the stochastic term error decreases with energy, the constant term will dominate at high energies. Note also that, since fo increases with energy, the e and pion response of the device will vary with E. Thus, if e/h is not = 1, the device will be nonlinear, and e/π response ratio will be energy dependent. Data collected from several calorimeters, including HF, is shown in Fig. 4. Clearly, devices with e/h ≠ 1 have an induced constant term which limits the resolution.

There is another energy nonlinearity which cannot be evaded even in a compensating device. At low energies, the hadronic content increases as E decreases because hadrons ionize with fewer hadronic interactions (threshold effects). Thus, the binding energy losses are reduced, leading to a low energy calorimetric nonlinearity[8]. Data on e/π and e/p are shown in Fig. 5, where the low energy, E < 3 GeV , nonlinearity is quite evident. Recall that for E < Et, no pions can be produced, so that the hadron only ionizes, and thus, e/h ~ 0.6.

2.5 Jet vs Single Particle Response

So far, the response of a calorimeter to individual particles has been examined. However, in particle physics the basic entities are quarks and gluons. Since they are confined, one is reduced to examining the "jets" of particles that are the evidence for that confinement. The response of a calorimeter to an ensemble of particles with a distribution of momenta is not trivially related to the single particle response. Suppose the jet (energy E) consists of a number of particles, n (<n> ~ ℓn(E)), distributed as D(z), where $k_i = z_i E$ is the individual particle momentum. Then, assuming a calorimeter with stochastic coefficient a and constant term b, the jet energy is measured with an error;

$$zD(z) = (1-z)^m, \quad m \sim 5$$
$$\sum_i k_i = E, \quad \sum_i z_i = 1 \qquad (11a)$$

$$dk/k = a/\sqrt{k} \oplus b$$
$$dE/E = a/\sqrt{E} \oplus b\sqrt{\sum_i z_i^2} \qquad (11b)$$
$$\sim a/\sqrt{E} \oplus b < z_1 >$$

Thus, the stochastic coefficient for the jet energy resolution is the same as the single particle coefficient, but the constant term is reduced. For the fragmentation function given in Eq. 11a, $<z_1> \sim 0.23$, and the reduction in the constant term can be quite large. Therefore, the e/h $\simeq$ 1 requirement on jets may be more relaxed than that for single particles, especially since jets themselves are rather ill defined objects.

3. Second Order Effects, Transverse Shower Development

The previous discussion assumed that the cascade particles moved only in one dimension along the direction of motion of the incident particle. As seen in Eq. 5, a high energy incident particle causes a 1-d cascade to lowest order. However, since the energy of the cascade particles degrades as one goes deeper into the shower, this approximation must inevitably break down.

3.1 Moliere Radius, Position Resolution

Clearly, the mean production angle in an EM cascade increases with depth. At the EM SM, using Eq. 5;

$$< \theta > \sim m_e / e(t) \sim m_e / Ec \qquad (12)$$

For example, in Pb, with Ec ~ 7 MeV, $<\theta>$ at SM is ~ 4°.

More critical is the multiple scattering of the cascade particles at the end of the shower. For e(t) ~ Ec, the multiple scattering in the last Xo defines the Moliere radius, r_M.

$$< Pt >_{ms} = Es\sqrt{t}, \quad Es = 21MeV$$
$$r_M = EsXo/Ec \sim \left[7(gm/cm^2)\right][A/Z] \qquad (13)$$

Thus, one expects that the EM shower begins, and persists, with a core of high energy cascade particles, surrounded by a halo of soft particles which scatter increasingly as the shower depth increases. At SM, the typical transverse EM scale is expected to be r_M. For example, in Pb, the Moliere radius is ~ 1.8 cm. The expected transverse distribution is shown in Fig. 6a.

For hadronic showers, a similar analysis leads one to expect that the hadronic component of the cascade at shower maximum will have angles defined by $<Pt>_\pi$ and Et.

$$< Pt >_\pi \sim 300MeV$$
$$e(\mathrm{v\,max}) \sim Et \sim < Pt >_\pi \qquad (14)$$
$$r_\pi \sim \lambda o$$

Since the transverse impulse, $<Pt>_\pi$, is comparable to the longitudinal shower energy/particle, Et, the transverse distance in going the last absorption length is comparable to λo.

Since there are EM and hadronic components of a pion induced cascade, Eq. 7, one expects that there are 2 characteristic transverse distance scales, r_M and λo. This behavior is observed in the data which is presented in Fig. 6b. Clearly, for EM showers the transverse scale is r_M, and the core and halo components exist, and widen with shower depth. For hadronic cascades there is an EM core and an hadronic halo.

The stochastic nature of the multiple scattering process leads one to expect that the position resolution capability of a calorimeter would scale as $1/\sqrt{E}$. The previous discussion raises the expectation that the hadronic resolution in transverse position will be worse than the EM, as seen in the data[9].

$$dx_t \sim 1\sqrt{E} \tag{15}$$

3.2 Multiple Scattering and Path Length

A finite angle for the cascade particles means that the traversal of the active sampling plates is not at normal incidence, as has been assumed so far. In fact, Monte Carlo studies[10] indicate that, in Pb, roughly 40% of the energy is deposited by e with energies < 1 MeV, and that this low energy component has a substantial probability to even be moving backwards with respect to the shower.

One can estimate the effect by replacing Δt in Eq. 9 by $\Delta t/<\cos\theta>$. The angle is estimated by assuming e(t) ~ Ec and <Pt> ~ Es. The increased path length effectively causes thicker sampling;

$$a \rightarrow a / \sqrt{\cos(Es / Ec\pi)} \tag{16}$$

For example, for Pb with 1/2 Xo sampling, $<\cos\theta> \sim 0.64$, leading to a 7.8% stochastic coefficent instead of the previously estimated 6.2%.

3.3 Ionization Fluctuations and Delta Rays

The previous approximation has been that each cascade particle leads to the deposit of a fixed amount of ionization energy, as given in Eq. 1b. The failure of normal incidence has already been mentioned. There are, in addition, fluctuations in the deposited ionization energy due to "Landau tails" caused by delta ray emission. Since these are elastic recoil electrons, they also result in very wide angle cascade components, with large path length fluctuations.

Clearly, these fluctuations are most important for "thin" active layers, where the energy loss in the active layer, δE, is << the energy loss in the absorber layers, ΔE. For gaseous or liquid detectors the stochastic term may be increased by up to 40% with respect to the previously discussed naive estimation[1].

4. Higher Order Effects in Sampling Calorimetry

There are many fine tuning effects in sampling calorimetry which require a detailed knowledge of energy deposition within the sampling layers. For example, a low energy photon will transfer energy to the medium by Compton scattering or the photo effect. Below ~ 1 MeV in

Pb the photoeffect, scaling as Z^5, dominates. The mfp for a 1 MeV photon in Pb is 3 cm, or ~ 6 Xo. Hence, a photon may cross several sampling layers, an effect as yet unexamined.

In this section, a few selected topics are mentioned which are of current interest and are under study at present.

4.1 Fine Sampling

Examination of Eq. 9 shows that, if the sampling frequency increases, the stochastic resolution decreases. Obviously, for fine sampling the approximation that all loss is in the passive absorber is invalid. Also, the approximation that the signal in successive active layers is uncorrelated becomes invalid. An approximate form for the stochastic coefficient is[1];

$$a \sim (1-R)\left[(\delta E + \Delta E)^{(1-R)/2}\right] \tag{17}$$

where R is the ratio of energy loss in the active to all layers, $\delta E/(\Delta E + \delta E)$. Note that as $R \to 0, \delta E \to 0$, and Eq. 9 is obtained as a limiting case.

The stochastic coefficient a is shown in Fig. 7 as a function of R. As expected from estimates given following Eq. 9, for R ~ 10%, a ~ 7% stochastic term is seen. However, as $R \to 1$, $a \to 0$ (see Eq. 17), as seen in Fig. 7. Fully active calorimeters, R=1, have energy measuring limitations, $a \neq 0$, which are not discussed here. Therefore, the R=1 limit is an artifact of the presumed form given in Eq. 17. Nevertheless, it is a reasonable representation of the data shown in Fig. 7 for sampling calorimeters.

4.2 Cladding and Compensation

A "classical" sampling device consists of high Z absorbers interleaved with low Z active layers. The shower development is largely determined by the absorber. In particular, the critical energy defines the end of multiplication, Ec ~ 1/Z. Cladding refers to surrounding the active layers with a low Z material. This layer has a higher Ec, which means the number of cascade particles will be reduced. Thus, the EM response, e in Eq. 2 , will be reduced. Obviously, only sampling calorimeters can achieve compensation by utilizating this reduction in e.

This effect has, indeed, recently been observed[11] in Si, warm liquids, and plastic. In plastic readout, a cladding of Al reduces e/π in Pb by ~ 10%, but in Fe by < 2%. This behavior is expected from the 1/Z scaling of Ec. The data on Fe and Pb with plastic readout are shown in Fig. 8. Clearly, the ability to "tune" e/π gives one an added degree of freedom in sampling calorimeters. For example, e/h=1 can be achieved in Fe calorimeters by judicious cladding.

4.3 Neutrons and Compensation

As discussed above, a calorimeter with $e/h \neq 1$ has a constant term in the energy resolution. For most calorimeters, the binding energy losses mean that $e/h > 1$. Thus, one must increase h or decrease e to achieve "compensation". In the previous section, the cladding method was discussed which allows one to achieve compensation by lowering e. As shown in Fig. 9, the various clad combinations lead to different constant terms. They are proportional to $|e/\pi - 1|$, with a proportionality of ~ 14%, in rough agreement with Eq. 10 and the subsequent discussion which estimated dfo.

The other avenue is, clearly, to increase h. The binding energy losses lead to many evaporation neutrons. Detection of the neutrons with a large effective sampling fraction is a way to

achieve compensation. Hydrogenous active materials are the standard way to increase neutron detection. One needs to go to a small sampling fraction, R, in order to maximize the fractional contribution of neutrons to the hadronic cascade signal. As discussed above, this leads to a poorer resolution, so that compensation and precision energy measurement are somewhat incompatible criteria. For example, a 2% sampling fraction in Pb is required for compensation, and Fig. 7 shows that this fraction is clearly not optimal for good resolution.

4.4 Calibration

Typically muons are used to supply a "mip" calibration point. Suppose there is a miscalibration or manufacturing error of each layer with a given rms. There is a shift in the mean, due to layers near SM being the ones involved in the brunt of shower detection, and an increase in the constant term as the medium is now nonuniform.

There are 2 ways to quantify the effects. A local calibration may be made, which means each tower is shifted in situ to have the correct mean, by using e.g. $Z \rightarrow ee$. A global calibration means that all towers are used without first calibrating in situ. These 2 methods yield "induced" constant terms which differ by a factor ~ 10, as shown in Fig. 10. This is true for both electrons and hadrons. Typically, for in situ local calibration, a 10% rms leads to acceptable constant terms. This sets the scale for manufacturing tolerances.

Other miscalibrations may come about due to external effects, such as external magnetic fields[13]. A nonuniform field makes the scintillator plastic active layers a nonuniform medium. Clearly, this effect also leads to an induced constant term[14].

4.5 Leakage, Hadronic Exit Weighting

Any real calorimeter is of finite length. Therefore, some cascade energy leaks out the back. The fraction leaking will be energy dependent, leading to an induced nonlinearity, and an increased rms error.

Possible alleviation of the problem comes from longitudinally segmenting the calorimeter in order to tag (and correct) late developing showers[15]. Another scheme is to "exit weight" the last characteristic length, ~ λo of the calorimeter. The higher exit weight preferentially samples late developing showers, leading to a correction to the shower energy. For example, the effect of hadronic leakage has been looked at in detail[2,16] for SDC.

4.6 Inert Material and Entrance Weighting, RADDAM

Often, calorimeters have material in front of them (beam pipes, tracking, magnet coils, cryostats). This inert material initiates cascades, and some energy is lost to the active layers. Since the longitudinal development of a cascade is energy dependent, a nonlinearity is induced, as well as an increased energy error[17].

One can try to restore the mean and the rms by "entrance weighting" the first active layer ("preshower or massless gap"). Basically, one is tuning the sampling fraction to be uniform by weighting the first layer. A study of HF data[18] is shown in Fig. 11. The linearity is restored to ~ 2% and the error reduced to < 1% at high energy, E > 100 GeV for 4 Xo of material in front of a Pb EM calorimeter. The optimal preshower weight is ~ 3.5.

A related situation obtains in the case where the calorimeter is damaged by radiation. That damage follows the e energy profile, Eq.6, so that the damaged device becomes nonuniform. The

inhomogenity induces a constant term. Typically, for 50% signal loss at shower maximum, a 40% nonlinearity is induced, and a 3% constant term[19].

The problem can be reduced by recalibration and the use of longitudinal segmentation. An e cascade has a shape given by Eq. 6; the main event by event fluctuation comes from the cascade initiation point. Longitudinal segmentation can be used to measure the initiation point and correct for nonuniformity. A factor of ~ 2 reduction can be obtained in the sensitivity to radiation damage when the optimal depth for the division between the 2 EM depth "compartments" is chosen[19]. Note that this method is feasible for isolated e and hadrons; for jets it is not practical.

A situation related to RADDAM is the occurrence of a broken layer readout. This problem has been studied[20] using the HF data set. For ~ 1/2 Xo Pb sampling, an EM calorimeter has a < 6% energy shift and an rms increase of < 12% if only 1 layer is broken. Clearly, the mean can be recalibrated, if the existence of the broken layer is known. A Fe calorimeter with 15% λo sampling has a < 5% energy shift and a < 20% rms increase. Clearly, the effect of any given layer is very dependent on the location in depth of the broken layer.

5. References

1.a C. Fabyan, Calorimetry in High Energy Physics, pg. 257, in Experimental Techniques in High Energy Physics, Ed. T. Ferbel, Addison-Wesley (1987).

1.b U. Amaldi, Fluctuations in Calorimetry Measurements, pg. 325, in Experimental Techniques in High Energy Physics, Ed. T. Ferbel, Addison-Wesley (1987).

1.c R. Wigmans, Advances in Hadron Calorimetry, Ann. Rev. Nucl. Part. Sci. 133 41 (1991).

1.d T.S. Virdge, Performance and Limitations of Electromagnetic Calorimeters, in Calorimetry in High Energy Physics, Ed. A. Ereditato, World Scientific (1992).

1.e J.E. Brau, Hadron Calorimetry--Optimizing Performance, in Calorimetry in High Energy Physics, Ed. D.F. Anderson et al., World Scientific (1991).

1.f P.B. Cushman, Electromagnetic and Hadronic Calorimeters, Vol. 9, in "Advanced Series on Directions in High Energy Physics, Ed. F. Sauli, World Scientific (1992).

2. A. Beretvas, et al., "Beam Tests of Composite Calorimeter Configurations from Reconfigurable-Stack Calorimeter", Nuc. Inst. Meth., A329, 50 (1993).

3. Review of Particle Properties, Phys. Rev. D45 (1992).

4. R.K. Bock, et al., CERN-EP/80-206 (1980).

5. R. Wigmans, High Resolution Hadron Calorimetry, Nucl. Inst. Meth., A265, 273 (1988).

6. R. Wigmans, on The Energy Resolution of Uranium and Other Hadron Calorimeters, Nuc. Inst. Meth., 389, A259 (1987).

7. D.F. Groom, pg. 59, in Proceedings of the Workshop on Calorimetry for the SSC, Ed. R. Donaldson, et al., World Scientific (1990).

8. A. Andresen, et al., Nucl. Inst. Meth. A290 93 (1990).

9. D. Acosta, et al., CERN PPE/91-11, CERN (1991).

10. G. Fisher, Nuc. Inst. Meth. 156, 81 (1978).

11. F. Lemeilleur, et al., Phys. Lett., B222, 518 (1989).

WALIC Collaboration, Studies of Compensation of Iron/TMP and Lead/TMP Sampling Calorimeters, LBL-33654 (1993), submitted to Nuc. Inst. Meth.

A. Beretvas, et al., Study of Homogeneous Absorber Materials and Low Z Cladding Layers in the Reconfigurable-Stack Calorimeter, to be submitted to Nuc. Inst. Meth.

12. Solenoidal Detector Collaboration, Technical Design Report, pgs. 6-20, SDC-92-101 (1992).

13. D. Blomker, et al., Nuc. Inst. Meth. A311, 505 (1992).

14. D. Green, "Magnetic Field Effects on Endcap EM Calorimetry in SDC", Fermilab-TM-1826 (1993).

15. D. Green, et al., "Depth Requirements in SSC Calorimeters", SDC-91-00016 (1991).

16. D. Green, Physics Requirements for LHC/SSC Calorimetry. in Calorimetry in High Energy Physics, Ed. A. Ereditato, World Scientific (1991).

17. D. Green, "SDC Preshower Depth and Weighting Factor Using Hanging File Data", Fermilab-TM-1829 (1993).

18. D. Green, " 'Massless Gap' Corrections to the SDC EM Energy Resolution", Fermilab-TM-1848 (1993).

19. D. Green, "Longitudinal Information and Radiation Damage in EM Calorimetry", Fermilab-TM-1828 (1993).

D. Green, et al., "Radiation Damage, Calibration and Depth Segmentation in Calorimeters", Fermilab-FN-565 (1991).

20. D. Green, "The Effect of Inoperative Readout Layers on SDC Calorimetry", Fermilab-TM-1855 (1993).

270 GeV pions

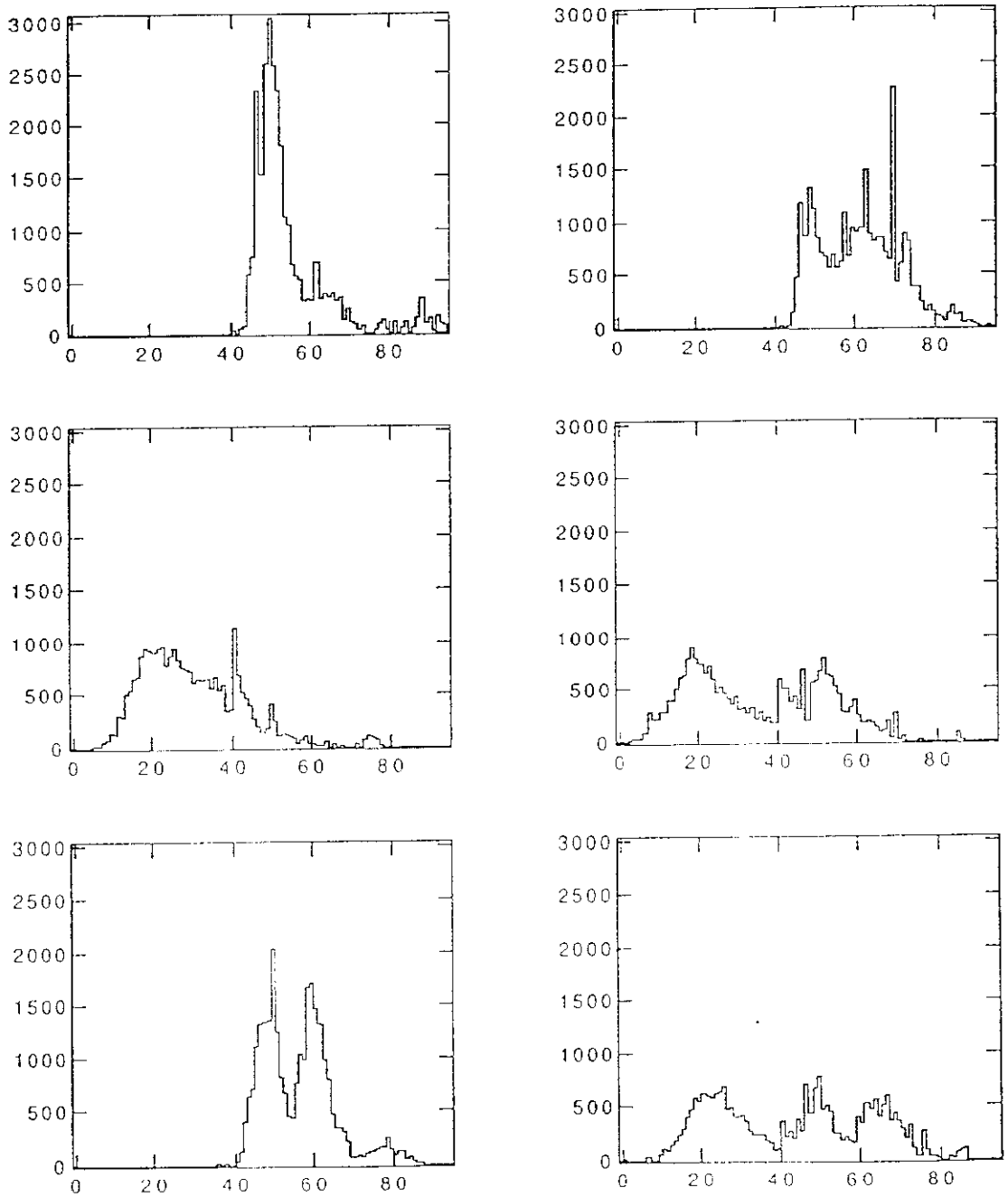

1. Depth profiles for individual 270 GeV incident pions. The HF stack consists of 40 plates of 1/8" Pb and 56 plates of 1" Fe.

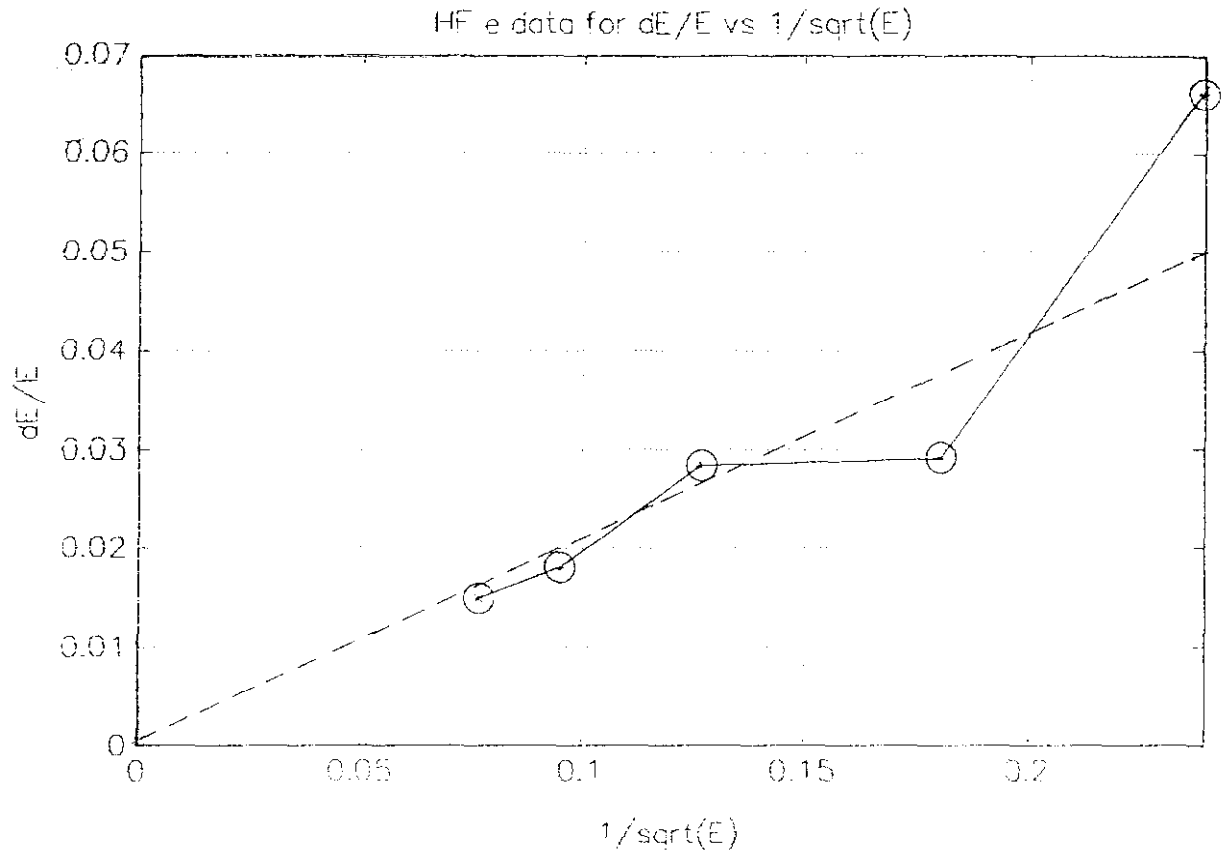

2. Data from HF incident e events. The fractional energy resolution, dE/E, is plotted as a function of $1/\sqrt{E}$.

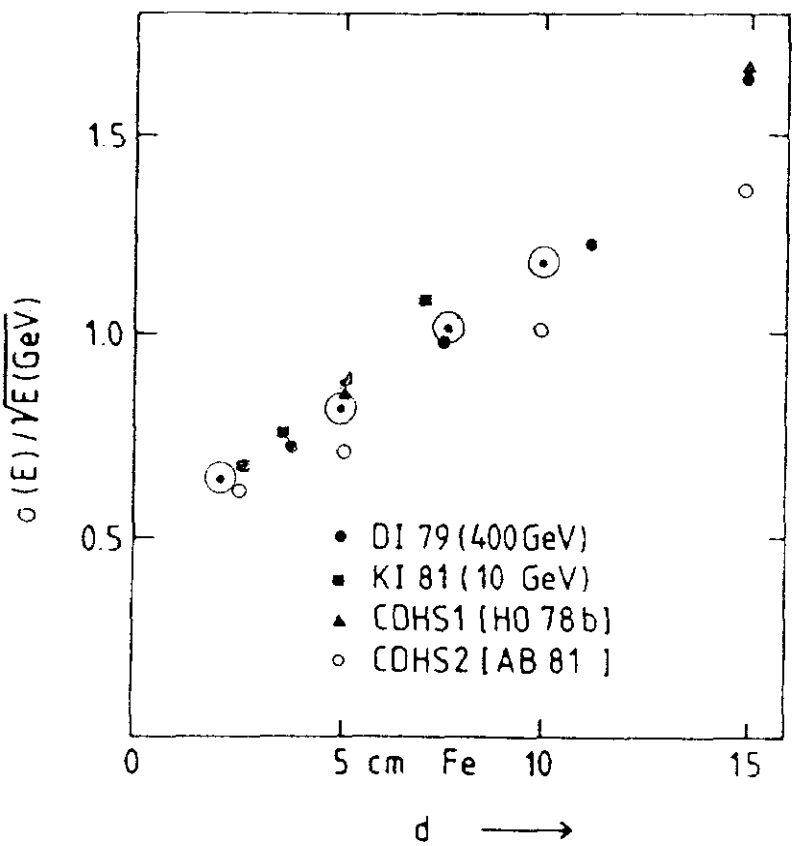

3. Data from HF incident h events. The stochastic energy term, $(dE/E)\sqrt{E}$ is plotted, in %, as a function of the sampling thickness for Fe calorimeters. A compendium of other data is included.

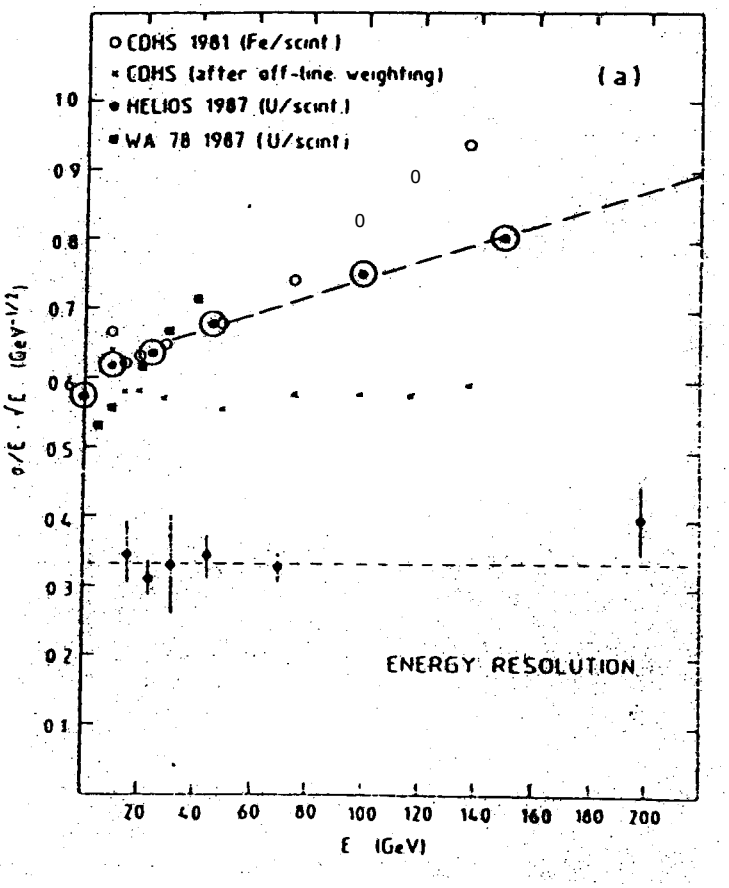

4. Collected data for calorimeters with different e/h responses. The response $(dE/E)\sqrt{E}$ is plotted as a function of E. Note that the HF data, with independent EM and HAD calibration, does not display as poor a constant term as the pure Fe CDHS calorimeter.

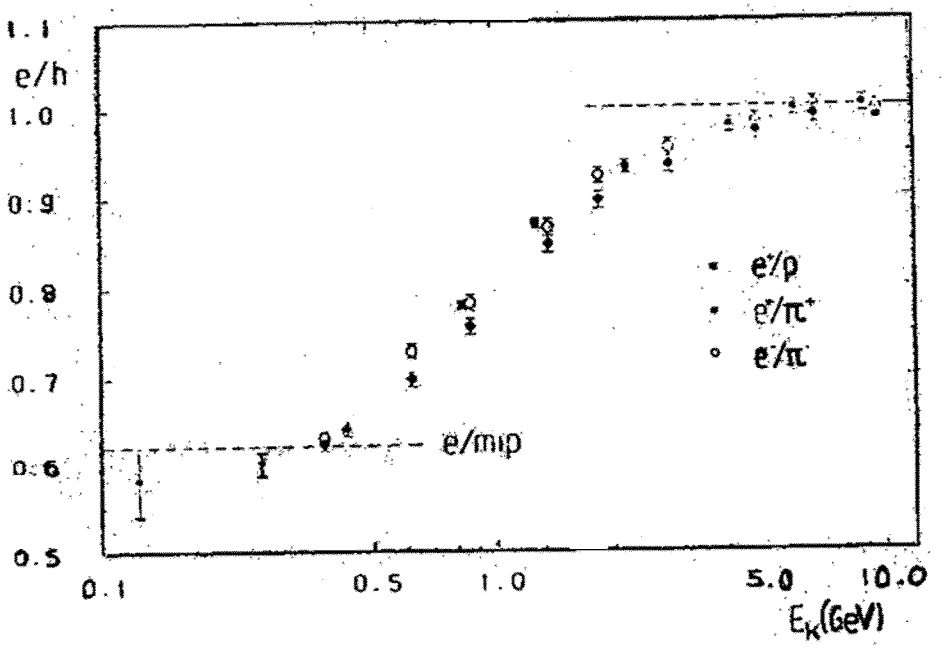

5. e/h as a function of E for low energy e and h. Note the nonlinearity of up to 40% at low energies.

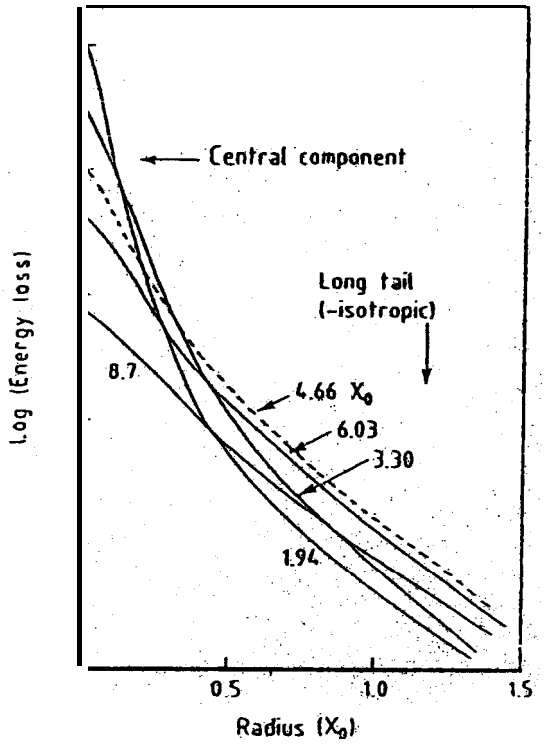

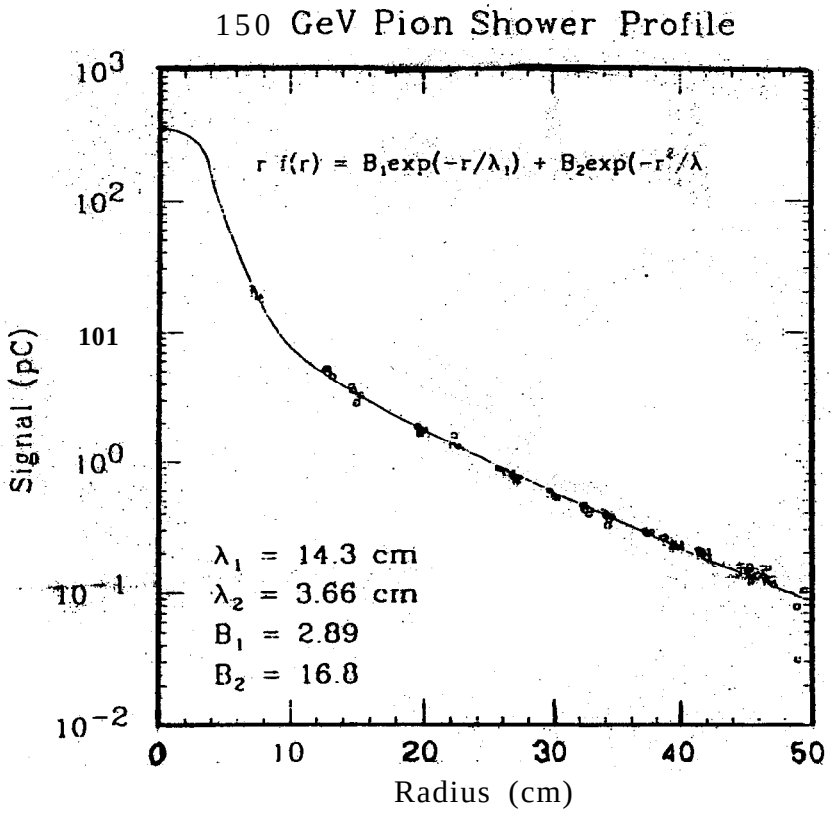

6. Transverse. **distribution** for e and h at various depths.
   a. Far the incident e, there is a central **core** and a long tail due to multiple scattering of e of **energy Ec** in the last X0 of path length.
   b. For the **incident** h, there is a central core and a long tail. The core is due to the EM component of the hadronically induced shower, **while** the tail is due to the hadronic component.

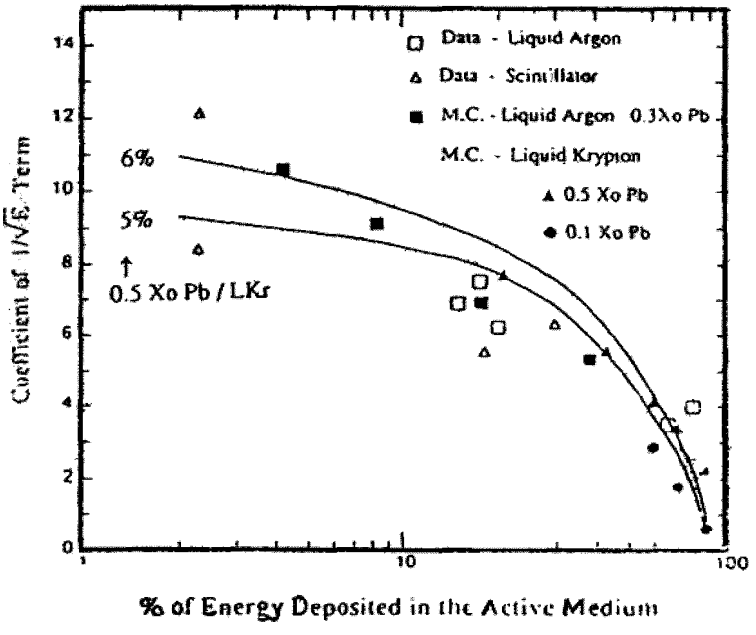

7. The effect of fine sampling calorimetry. The stochastic term coefficient is plotted as a function of the percentage of energy deposited in the active medium, the sampling fraction $R = \delta E / (\Delta E + \delta E)$.

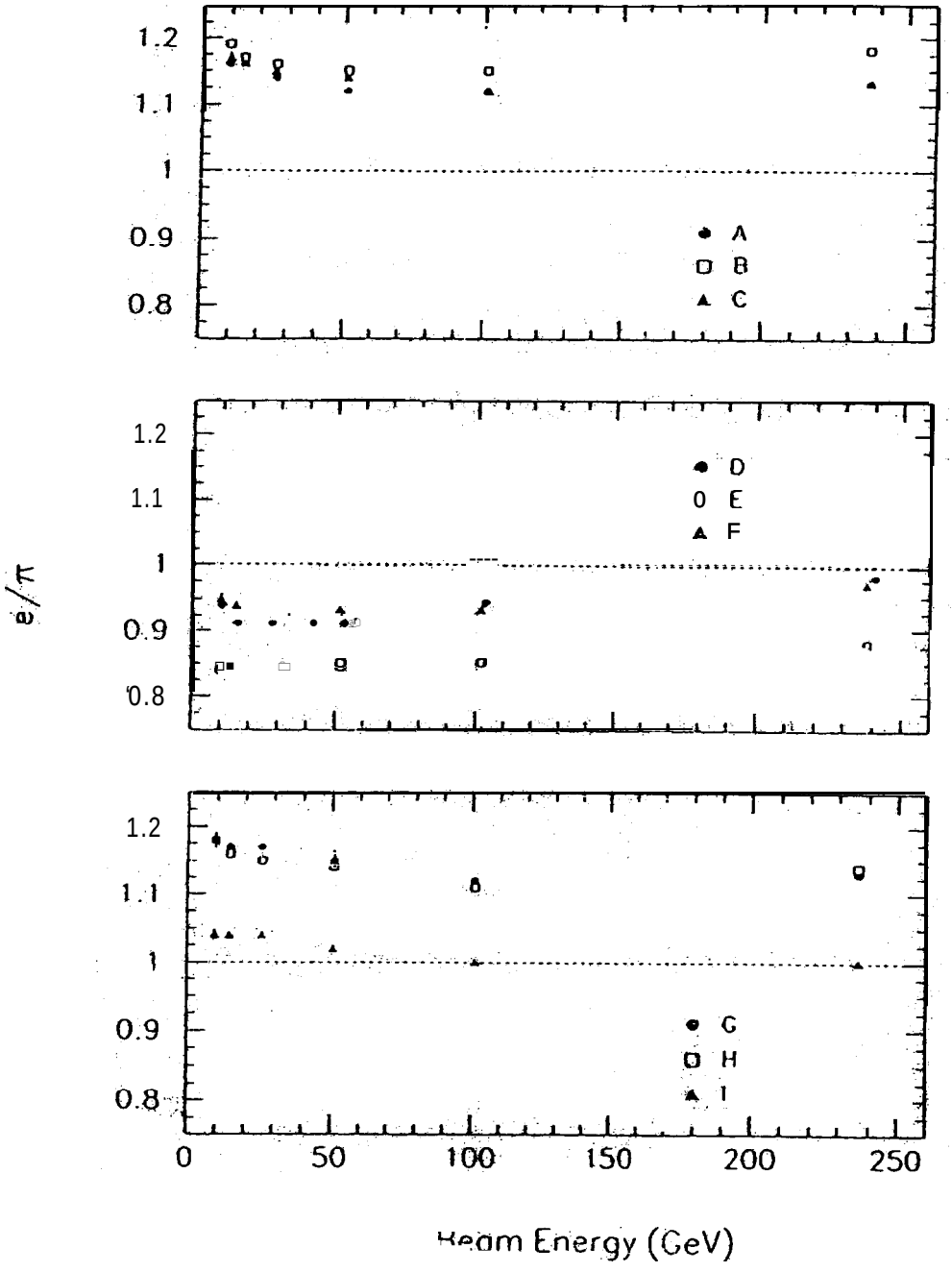

8. **The e/π ratio as a function of energy for clad Pb and Fe calorimeter configurations. The data are from HF cladding test configurations. Note the nontrivial energy dependence.**

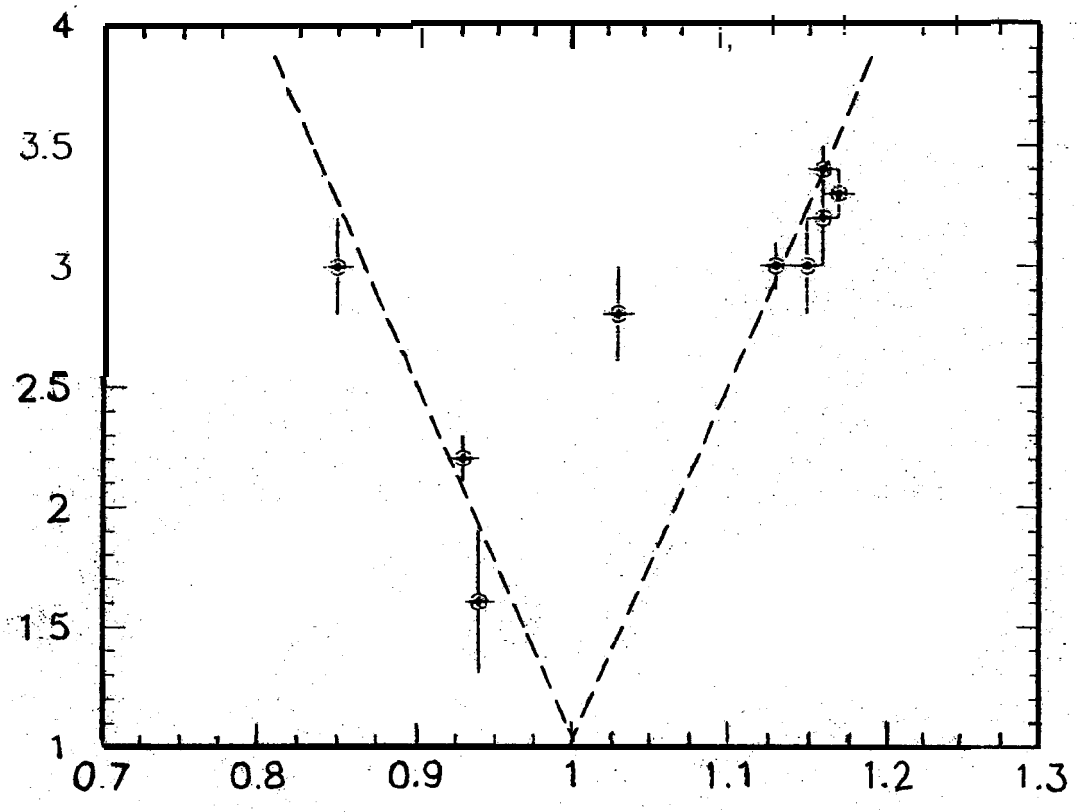

9. The constant term for various HF clad configurations as a function of the e/π response of the configuration. The rough dependence is that $b \sim |e/\pi - 1|(14\%)$.

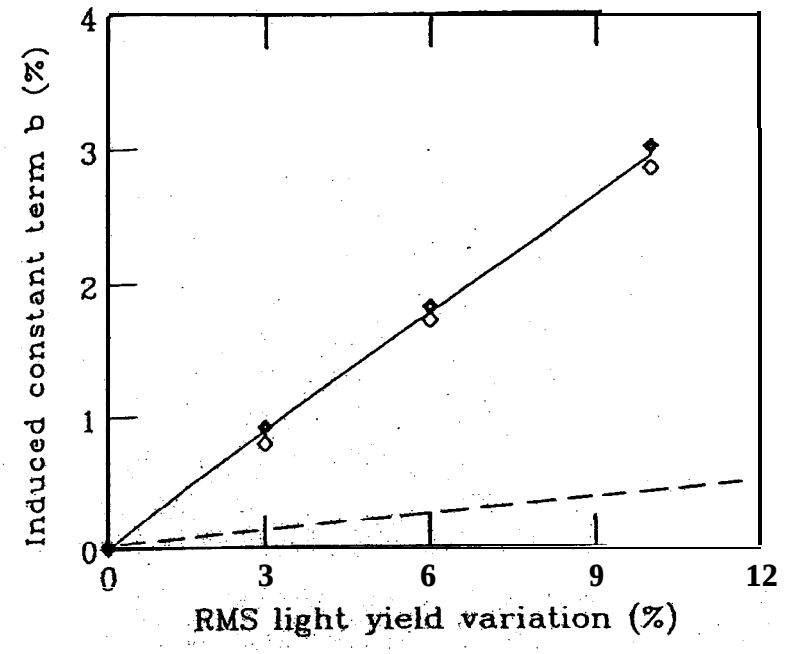

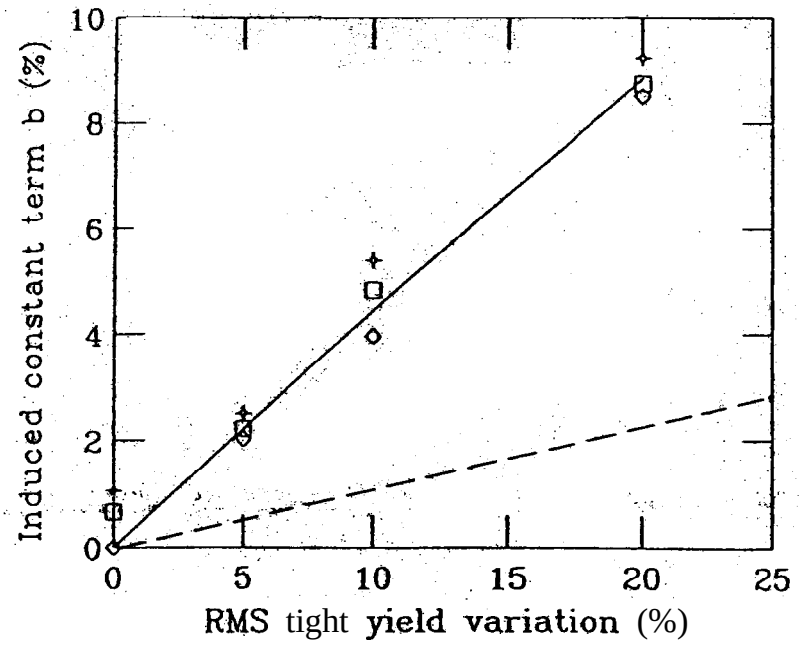

10. Induced constant term, b, as a function of the rms of the miscalibration for both global and local (equalized mean) calibration schemes. Notes that local, in situ, calibration implies a much reduced sensitivity to calibration and manufacture-errors.'
    a. HF and "Lab E" hadronic test data.
    b. HF data and EGS estimation.

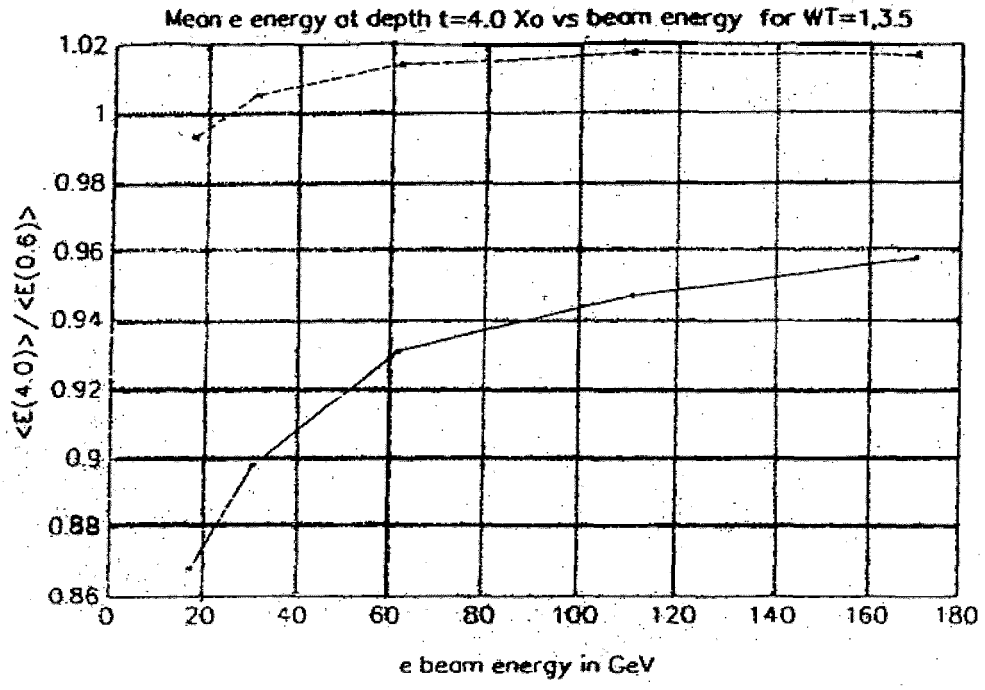

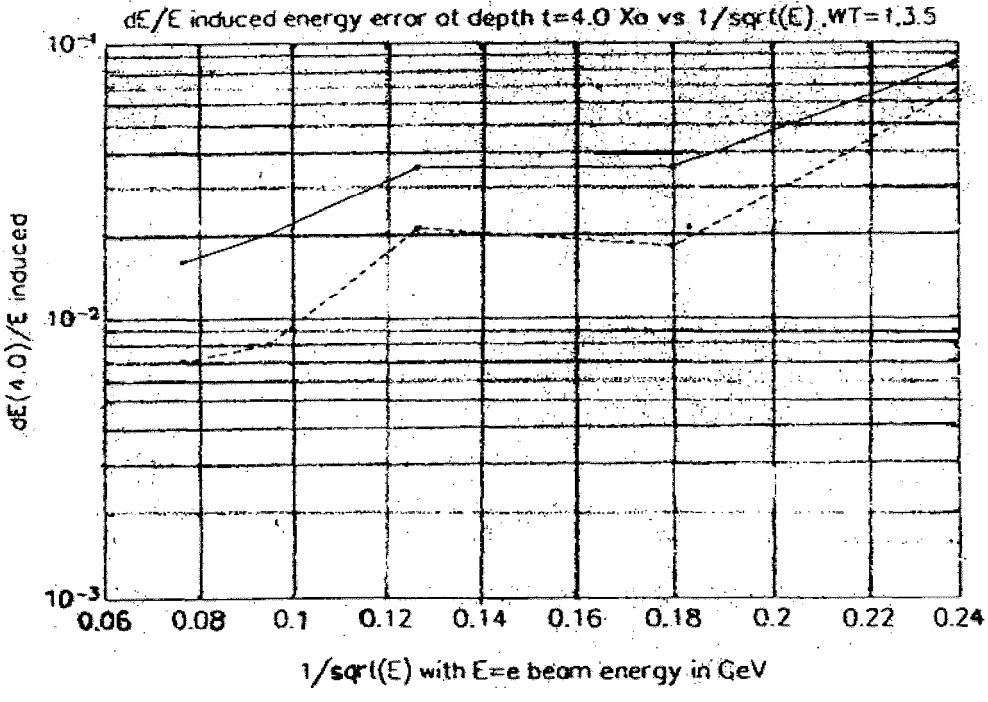

11. a. The mean EM energy observed in the HF calorimeter stack at a fixed depth of t=4.0 Xo and with fixed weights = 1, 3.5 as a function of incident e energy, E. The mean is scaled to the mean at t=0.6.
    b. The rms EM energy observed in the HF calorimeter stack at a fixed depth of t=4.0 Xo and with fixed weights =1 and 3.5 as a function of $1/\sqrt{E}$.